A Study of Power Distribution System Fault Classification with Machine Learning Techniques

Nicholas S. Coleman, Christian Schegan, and Karen N. Miu
Department of Electrical and Computer Engineering, Drexel University
Philadelphia, PA, USA
coleman@drexel.edu, cms68@drexel.edu, miu@coe.drexel.edu

***Abstract*—Power system protection includes the process of identifying and correcting faults (failures) before fault currents cause damage to utility equipment or customer property. In distribution systems, where the number of measurements is increasing, there is an opportunity to improve fault classification techniques. This work presents a study in fault classification using machine learning techniques and quarter-cycle fault signatures. Separate voltage- and current-based feature vectors are defined using multi-resolution analysis and input to a two-stage classifier. The classifier was trained and tested on experimental fault data collected in Drexel University's Reconfigurable Distribution Automation and Control (RDAC) software/hardware laboratory. Results show: (1) non-linear, and even non-contiguous decision regions on a "fault plane", using a phase voltage-based feature, and (2) an accurate classifier for determining the grounding status of multi-phase faults, using a neutral current-based feature.**

Keywords – fault classification; machine learning; power distribution systems; power system protection

I. INTRODUCTION

Fault detection and location are critically important procedures in power system protection and service restoration. Successful detection and location allows for the proper operation of protective relays, which isolate faults to temporarily de-energize faulted sections of the grid. Fault detection and location techniques in distribution systems have been studied extensively; some examples include [1]-[5].

This work considers fault *classification*. Fault classification answers the question: given that a fault has occurred, what type of fault has occurred? Accurate real-time fault classification can support superior grid operation by reducing the likelihood of relay operations on non-faulted phases. Dispersed measurement devices in smart distribution grids make online fault classification a feasible goal.

This work uses machine learning techniques to develop a fault classifier. A first step in machine learning is to characterize features of data sets. As such, it is noted that wavelet decomposition has been demonstrated to be an effective technique for generating features from the voltage and current waveforms observed during power system events and disturbances, as evidenced by [1]-[2], [6]-[12]. Wavelet transformation methods provide time-localization of spectral components and a multi-resolution decomposition of the transformed signal. In [1]-[2], continuous wavelet transforms were used to detect and physically locate faults in distribution systems. Wavelet-based detection of common transient power quality disturbances, such as transformer or capacitor energization events, was presented in [9].

Several works have successfully applied a variety of classifiers to the wavelet-generated features, including fuzzy-logic techniques [6], k-nearest neighbors [8], and neural networks [8]. The classifier in [7] maps wavelet coefficients to a normalized "fault triangle" or "fault plane", in which decisions regions were defined based on assumed likelihood in an ideal transmission system. Simulations validated the chosen regions on the fault plane, and success was demonstrated with experimental transmission system fault data as well. With this example for transmission systems, this paper investigates machine learning techniques for power distribution systems. Distribution system fault classification, however, can be a more difficult task, as the assumptions often used in transmission system analysis break down.

In particular, in order to better understand the impacts of unbalanced systems and real vs. simulated data on classifiers, this study uses experimentally obtained, short-circuit fault signals collected in Drexel University's Reconfigurable Distribution Automation and Control Laboratory (RDAC) [13] under a variety of unbalanced loading conditions. The fault signals, which are a subset of those collected in [11], include voltage and current waveforms measured at the feeder bus. It is noted that in this work, particular attention has been paid to multi-phase faults vs. single-phase faults: e.g. line-to-line (LL) and line-to-line-to-ground (LLG) faults.

The general feature generation and classification procedure adopted is as follows: 1) Daubechies wavelet transformations are used to generate features from phase voltage and neutral current waveforms; 2) three nonlinear support vector machine (SVM) classifiers are trained to identify faulted phases using normalized phase voltage features; 3) a perceptron classifier identifies fault grounding status with neutral current features. This study will demonstrate that:

- practical distribution systems yield highly non-linear decision regions on a "fault triangle",
- multi-stage machine learning techniques may be needed for actual power system applications.

II. MACHINE LEARNING APPROACH

Machine learning for power system protection begins with sampling real-time bus voltage and line current waveforms at each phase and on the neutral wire. The techniques used in this paper are now briefly reviewed.

A. Feature Generation

Individual phase voltage data is used to identify which combination of phases that experienced fault events. In addition, the neutral current is included to differentiate between

grounded and ungrounded faults. Features are generated from these sampled waveforms are transformed using a discrete time wavelet transformation (DWT) with, in particular, the Daubechies-4 (db-4) mother wavelet. The specific choice of db-4 is attributed to its known effectiveness with extracting features from available data [11].

B. *Linear Perceptron Algorithm*

Classifying faults as grounded or ungrounded falls under the basic category of perceptron classifiers. Consider the two-class case: feature vectors $\mathbf{x}_i \in \mathbb{R}^d$, $i = 1,...,n$, are generated from data points that belong to one of two true classes, ω_1 or ω_2. Using a training set extracted from the data, a perceptron algorithm trains a $d-1$ dimension decision hyperplane, $\mathbf{w}^{\mathbf{T}}\mathbf{x} + w_0 = 0$ by tuning the weights w_j, $j = 0,...,d$, where $\mathbf{w} = \begin{bmatrix} w_1 & \dots & w_d \end{bmatrix}$.

The algorithm will minimize the number of misclassifications on the training set, quantified by a cost function $J(\mathbf{w})$:

$$J(\mathbf{w}) = \sum_{x \in Y} \left| \mathbf{w}^{\mathbf{T}}\mathbf{x} + w_0 \right| \tag{1}$$

where Y is the set of misclassified training data. Typically, a gradient descent method on $J(\mathbf{w})$ is used to find the optimal decision hyperplane. If ω_1 and ω_2 are not entirely linearly separable, then the linear perceptron cannot achieve errorless classification. Even though this is the case, a perceptron algorithm can still tune a good classifier in many cases where the class overlap is mild. As such, the perceptron algorithm serves as a simple baseline against which to compare other, more complex classifiers.

C. *Support Vector Machines*

It is noted that the linear perceptron algorithm may not provide a unique solution. Consider Fig. 1 which illustrates a case of two linearly separable classes. Many hyperplanes attain $J(\mathbf{w}) = 0$; for example: both the solid and dashed lines provide total class separation of the illustrated training set, so either line is a solution for the perception algorithm. It may be of interest, however, to select a decision boundary that maximizes the margin between itself and neighboring members of the training set (in this case, the dashed in line in Fig. 1 is preferred).

Support vector machines (SVMs) maximize this margin between the decision hyperplane and vectors from either class [14]. The optimization problem solved to obtain the unique linear SVM classifier is:

$$\min J(\mathbf{w}, w_0) = \frac{1}{2}\|\mathbf{w}\|^2 \tag{2}$$

$$\text{s.t. } y_i(\mathbf{w}^T\mathbf{x}_i + w_0) \geq 1, \quad i = 1,...,n \tag{3}$$

where $y_i = 1$ if $\mathbf{x}_i \in \omega_1$, or $y_i = -1$ if $\mathbf{x}_i \in \omega_2$. Constraint (3) enforces a positive margin; weights can be scaled to satisfy this. For handle cases where the classes are not inherently linearly separable, a nonlinear SVM method is available. With a nonlinear SVM, feature vectors are mapped into a higher-dimensional space in which they are linearly separable (or at least more linearly separable than in their native vector space) [14]. This mapping is achieved through the kernel trick; this work uses a Gaussian radial basis function for the kernel.

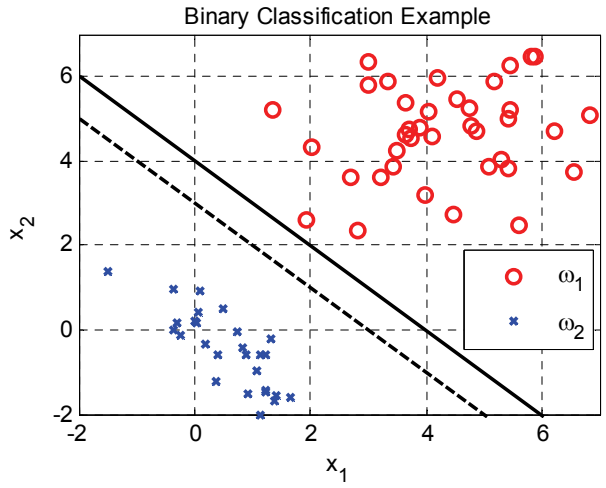

Fig. 1. Binary classification example. While both lines achieve $J(\mathbf{w}) = 0$ in the perception algorithm, the dashed line provides a larger margin between the decision boundary and the training set data points.

III. Classifier Design

A. *Feature Generation*

v_a, v_b, v_c and i_n were used to generate features. Voltage-based features were used to identify phases affected during fault events. The neutral current-based featured was used to differentiate LL and 3P faults from LLG and 3PG faults. For each of these sampled waveforms, DWT coefficients were obtained using MATLAB's Wavelet Toolbox. These coefficients require additional manipulation in order to extract suitable features. Each fault event, j, is associated with two feature vectors that stem from the DWT coefficients:

- $E^j \in \mathbb{R}^3$, which contains information about the three phase voltages, and
- $F^j \in \mathbb{R}$, which contains neutral current information.

$E^j = [E_A^j \quad E_B \quad E_C]^T$ contains normalized coefficient "energies" that are effectively projections of the data onto a fault plane [7]; this concept will be visited in the next section. For fault event j, E^j is computed from windowed groupings of four consecutive second-voltage-detail coefficients, V_p^{D2}. At the second-detail level, this window corresponds to 16 samples of v_p, or one-quarter cycle of the voltage waveform.

Fig. 2 illustrates the transformation from sampled voltage data to the pre-normalized, per-phase energy coefficients, e_{va}, e_{vb}, e_{vc} during a line-to-line A-to-C fault. These pre-normalized phase energies are then normalized to the fault plane in E-space, where they sum to unity, and form E^j. $F^j \in \mathbb{R}$ is computed for event j by summing the magnitudes of the following wavelet coefficients at index k:

$$F^j = \left| I_n^A[k] \right| + \left| I_n^{D4}[k] \right| \tag{4}$$

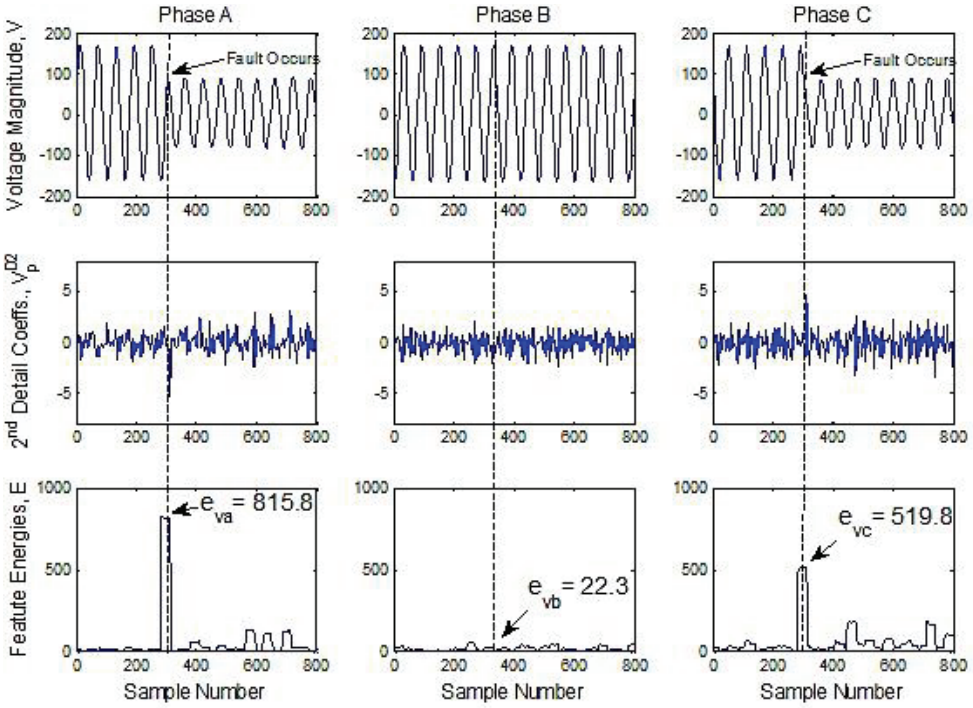

Fig. 2. Sample generation of the voltage-based feature vector, E^j, for a line-to-line A-to-C fault created in the RDAC Laboratory. Observe that the energy values amplify the feature saliency observed during a fault. For the unfaulted phase B, the energy values are small.

Fig. 3 illustrates the generation of F^j for ABC and ABCG fault events. Please note the scales. The feature value associated with the grounded fault is much greater than the feature value associated with the ungrounded fault; the distinction is more extreme when comparing LL and LLG faults.

For the remaining discussion, the symbols E and F refer to their entire respective feature spaces. Figs. 4, 5, & 6 illustrate the fault feature spaces and the true labels for fault events collected in the RDAC laboratory: Figs. 4 & 5 include 758 events in E; Fig. 6 includes 551 events in F.

B. Classification Stage I: Supervised Classification of E - "Phase Voltage Features"

In Stage I, data from E is supplied to a series of binary SVMs to identify faulted phases for each event, regardless of whether the fault was grounded. Ignoring grounding, there are

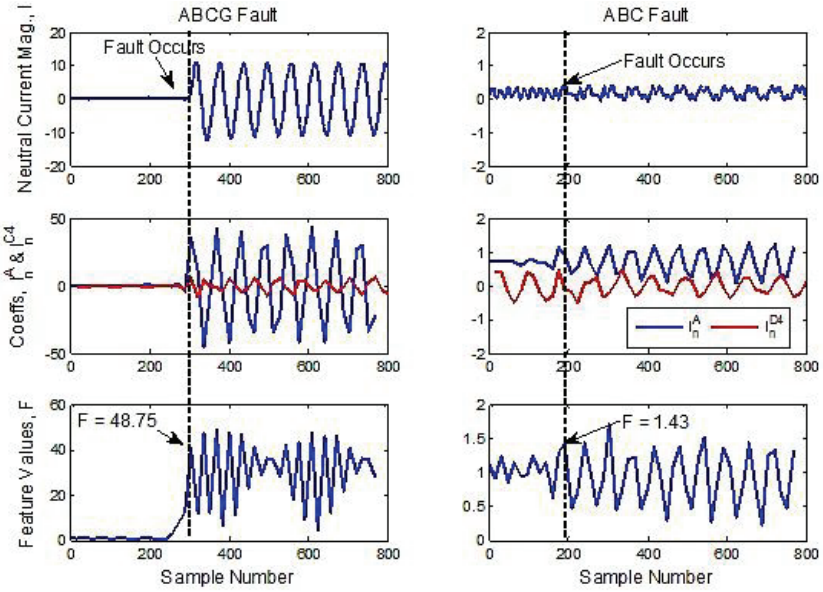

Fig. 3. Sample generation of the current-based feature, F^j, for ABCG and ABC faults. Note the scales. Two different loading conditions are represented.

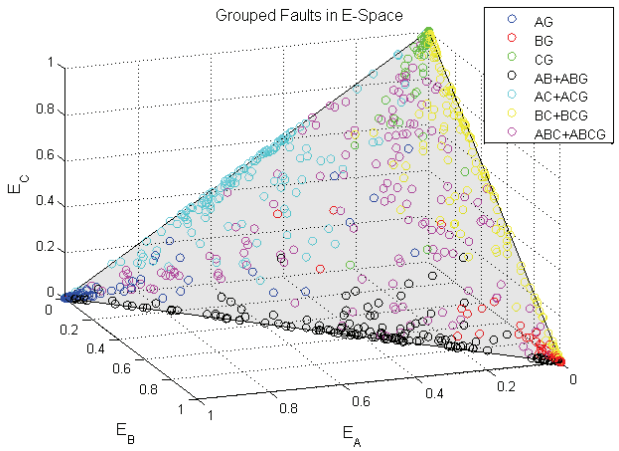

Fig. 4. (758) events in feature space E (the fault plane), grouped to distinguish between the existence of a fault conditions on each phase (i.e. grounding status not differentiated).

seven combinations in which one or more phases are faulted. Fig. 4 shows the true class label for 758 fault events on the fault plane. A clustering pattern is apparent in the feature space, but the groups are clearly inseparable. Therefore, instead of considering each combination of faulted phases (e.g. A, AB, ABC, etc.) as its own group, consider three separate classifiers that address each phase separately. For example, each subplot in Fig. 5 contains the same data set shown in Fig. 4, but events are labeled differently; red highlights data points that are faulted on the indicated phase. Each red group is equivalent to the union of four different groups from Fig. 4.

The faulted vs. unfaulted distinction, illustrated in Fig. 5, provides better class separability than the grouping the Fig. 4. Therefore, a three-SVM-ensemble used the data from E to learn three separate nonlinear decision boundaries (one for the status of each phase). The overlay of these three decision boundaries divide E into various partitions that correspond to the AG, BG, CG, AB(G), AC(G), BC(G), and ABC(G) groups. For coding purposes, the output of Stage I is a three-bit binary sting where a 1 indicates a faulted phase. A fourth bit is added in the next subsection, which considers current features, F, to form a four-bit binary output for each fault event, which maps to a unique fault class.

C. *Classification Stage II: Supervised Classification of F, "Current Features"*

Considering F as a separate feature space greatly reduces the computational complexity and data density required to build a classifier. Since this work focuses on short-circuit faults, faults identified in Stage I as single-phase are classified as LG and automatically assigned a fourth bit of 1, indicating grounding. Stage II processes the remaining events which are shown in F-space in Fig. 6.

In Fig. 6, a horizontal linear decision boundary separates nearly all of the grounded (red) fault events from the ungrounded (blue) fault events. Stage I handles the separation of LL(G) faults from 3P(G) faults, so separability between these groups is not required in Stage II. Because this data is truly one-dimensional, a single point F_b, selected by a

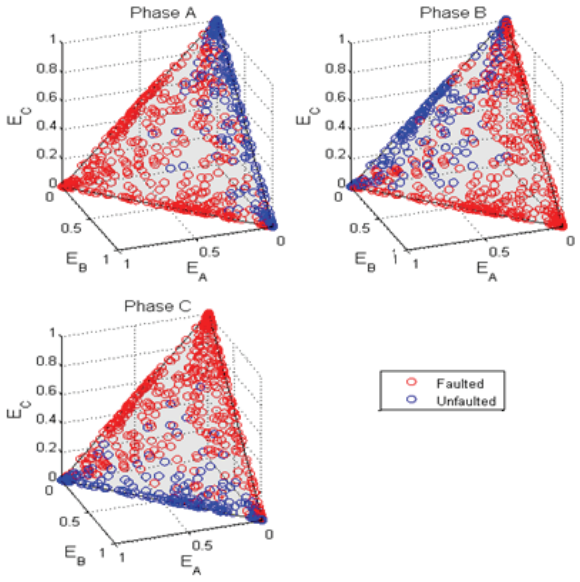

Fig. 5. (758) events in feature space E (the fault plane), grouped according to whether each phase was faulted (red) or not (blue).

perceptron with the goal of minimizing error in the training data, separates the grounded and ungrounded faults. Thus a fault event j with $F^j \geq F_b$ was classified as LLG or 3PG.

The output of Stage II is a fourth bit, which is 1 if for a fault classified as grounded and 0 otherwise. For each event, the cumulative result of Stages I and II is a four-bit binary string, "ABCG", containing 1's on the faulted phases A, B and/or C, and on G if the fault is grounded.

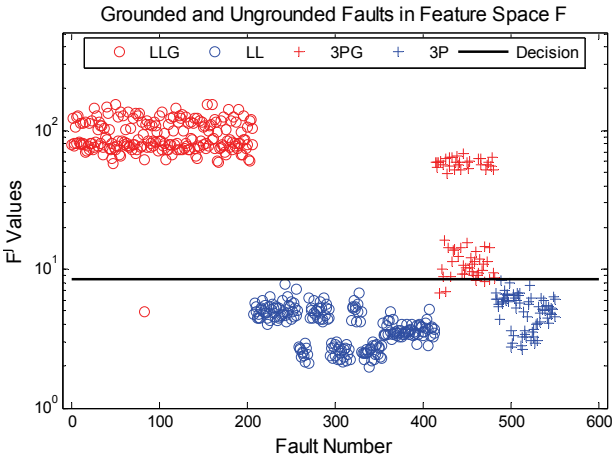

Fig 6. (551) LL(G) and 3P(G) events in feature space F, grouped by fault type. Note the logarithmic scale. The black line is the learned decision boundary.

IV. Study Results

A. *Test Circuit and Fault Data*

Fig. 7 illustrates the three-phase, nine-bus RDAC test circuit. The circuit is energized by utility power through an autotransformer to allow consistent voltage regulation at ~110±1 V at the feeder bus, where voltage and current measurements are taken. Light bulb banks are used for resistive loads to model residential or commercial loads; inductor banks

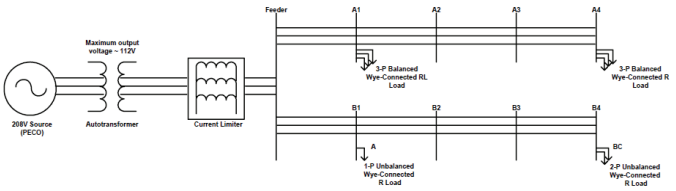

Fig. 7. Test circuit line diagram with sample load setting (multi-phase unbalanced). Faults were created on various buses [11].

were added to create series RL loads to mimic motor loads with a power factor of 0.898 lagging [11].

The RDAC laboratory allows for multi-phase loads to be connected at any of its nine buses. In addition, a set of 11 faults types (e.g. ABCG, AG, BC, etc.) can be created at any of the nine buses. The loads illustrated in Fig. 7 represent one of several load settings used throughout the experiments. In order to develop robust classifiers that can handle a realistic range of system conditions, for each fault type, a variety of "typical" load levels, load locations, and fault locations were used. Note that the phase angle at fault inception was not controlled in this experiment, further diversifying the fault events in the data set. Table I gives a brief outline of the various loading condition and fault events used in this study. Each of the 758 fault signatures in the data set includes time-varying voltage and current waveforms, sampled at 3.6 kHz (60 samples per cycle).

Table I. Loading conditions. A,B,C indicate phases with resistive loads of the specified Ω/phase. "M" indicates 3-phase motor load of 40+j19.599 Ω/phase. Bus B3 is omitted because it was never loaded. "Count" indicates the number of times each loading condition was subjected to *each* of the 11 fault types (*exception: only 11 faults of type ABCG recorded).

Condition	Count	Load Locations						
		A1	**A2**	**A3**	**A4**	**B1**	**B2**	**B4**
Low (200 Ω/ph.)	12	M			ABC	A		BC
	8				M	C	ABC	AB
Medium (66.7 Ω/ph.)	12	M			ABC	A		BC
	8				M	C	ABC	AB
Heavy (40 Ω/ph.)	12*	M			ABC	A		BC
	8				M	C	ABC	AB
Balanced (40 Ω/ph.)	1		M		ABC			ABC
	2		ABC	M				ABC
	3	ABC			ABC		M	
	3	ABC				ABC		M

B. *Two-Stage Classifier*

Of the 551 LL(G) or 3P(G) fault events, 165 were randomly selected to train Stage II (~30% of the multiphase faults). Of the 593 events not in the Stage II training set, 227 were used to train Stage I (~30% of the full data set). This left 366 fault events for testing at the beginning of Stage I. Table II summarizes the classifiers and their parameters.

Fig. 8 illustrates the ensemble's non-linear decision regions on the fault plane. The three SVMs were trained with actual data, thus naturally including measurement inaccuracies, in Stage I. It is noted that the decision boundaries are distinctively non-conforming to the "ideal" decision regions used in [7]. This highlights an area of future work with respect to resolving the sensitivity of decision boundaries to data sensed within measurement accuracy bounds.

Table II. Selected classifiers and their parameters.

	Stage I	**Stage II**
Goal	Identify faulted phase(s)	Identify if the fault is grounded
Classifier Type	Ensemble of three binary, non-linear support vector machines	Linear perceptron
Classifier Parameters	Kernel: radial basis function (RBF); RBF Parameters: scaling factor: 0.01; penalty factor: 1000; convergence tolerance: 1e-8	Cost function: minimize training data error
Training Data	227 feature vectors in E, randomly selected from the 758 total events (~30%)	165 features in F, randomly selected from the 551 LL(G) and 3P(G) faults (~30% of 551)
Testing Data	366 fault signatures (disjoint from both training sets, ~48% of 758 total). Note that if Stage I identifies only one phase as faulted, then Stage II automatically chooses "grounded"	

Considering the classifier stages separately, Stage I had a pure accuracy of 66.9% (121 errors in 366 events) in determining faulted phases, and Stage II had a pure accuracy of 98.4% in identifying grounding (6 errors). These results reflect the significant group overlap in Fig. 4 (E-space), and relative separability of groups in Fig. 5 (F-space). In Stage II, the one-dimensional decision boundary was placed at $F_b = 8.478$. The overall classification accuracy was 66.7% on the testing data (122 errors); Table III shows the classifier output matrix.

1) *Remarks*

- Distinguishing between grounded and ungrounded faults may actually be "easier" in real systems compared to in simulated systems, because properly selected ground current-features are more salient during real fault events than during simulated fault events.
- The learned decision regions in the fault plane are non-contiguous and non-convex. This is a reflection of complexity added to the fault classification problem when working with real data; the impacts of measurement inaccuracy must be further studied.

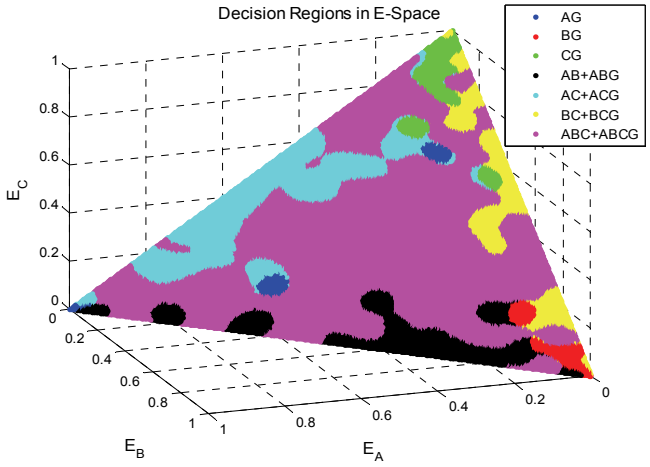

Fig. 8. Non-linear decision regions in E-space defined by the three SVM ensemble with the Stage I training data (227 of 758 cases, randomly selected).

Table III: Classifier output matrix for the fault classification experiment.

True Class \ Classifier Output	AG	BG	CG	AB	AC	BC	ABG	ACG	BCG	ABC	ABCG	Total	*Acc.*
AG	33	0	0	0	0	0	3	0	0	0	7	43	*76.7%*
BG	0	32	0	2	2	0	0	0	3	0	2	41	*78.0%*
CG	3	0	19	0	0	0	0	0	0	8	0	30	*63.3%*
AB	7	3	0	10	0	0	0	0	4	0	1	25	*40.0%*
AC	1	0	0	0	31	0	3	0	0	1	2	38	*81.6%*
BC	1	0	0	1	0	22	0	0	0	11	0	35	*62.9%*
ABG	2	0	0	0	1	1	27	0	0	0	5	36	*75.0%*
ACG	0	0	0	0	0	0	0	16	0	11	0	27	*59.3%*
BCG	0	4	0	0	3	0	0	0	23	0	1	31	*74.2%*
ABC	2	0	5	1	0	2	0	5	0	14	0	29	*48.3%*
ABCG	4	2	0	3	1	0	1	0	2	1	17	31	*54.8%*
Total	53	41	24	17	38	25	34	21	32	46	35	366	
Acc.	*62.3%*	*78.0%*	*79.2%*	*58.8%*	*81.6%*	*88.0%*	*79.4%*	*76.2%*	*71.9%*	*30.4%*	*48.6%*		*66.7%*

V. Conclusions

This work presented a DS fault classification study, including wavelet-based feature generation and an ensemble classifier trained and tested on a set of 758 experimental quarter-cycle fault signatures. Using the popular db-4 wavelet to generate features, the Stage I classifier produced highly complex decision boundaries in the fault plane (Fig. 8). This study suggests that wavelet-based features are very sensitive to the effects of system imbalance present in distribution systems and real-time measurement error in practical distribution systems. The Stage II classifier successfully distinguished between LL/3P and LLG/3PG faults with 98.4% accuracy. Many existing fault classification procedures lack accurate methods for discerning grounding status, but because the Stage II classifier requires only neutral current measurements, it can be easily incorporated into existing classifiers to improve overall accuracy.

Acknowledgments

The authors gratefully acknowledge Dr. Andrew Cohen of Drexel University, Department of Electrical and Computer Engineering, for his feedback on this study.

References

[1] A. Borghetti, M. Bosetti, M. Di Silvestro, C. A. Nucci and M. Paolone, "Continuous-Wavelet Transform for Fault Location in Distribution Power Networks: Definition of Mother Wavelets Inferred From Fault Originated Transients," Power Systems, IEEE Trans. on, vol. 23, no. 2, pp. 380-388, May 2008.

[2] A. Borghetti, M. Bosetti, C. A. Nucci, M. Paolone and A. Abur, "Integrated Use of Time-Frequency Wavelet Decompositions for Fault Location in Distribution Networks: Theory and Experimental Validation," Power Delivery, IEEE Trans. on, vol. 25, no. 4, pp. 3139-3146, Oct 2010.

[3] R. H. Salim, M. Resener, A. D. Filomena, K. R. C. de Oliveira and A. S. Bretas, "Extended Fault-Location Formulation for Power Distribution Systems," Power Delivery, IEEE Trans. on, vol. 24, no. 2, pp. 508-516, Apr 2009.

[4] S. M. Brahma, "Fault Location in Power Distribution System with Penetration of Distributed Generation", IEEE Trans. Power Delivery, vol. 26-3, pp. 1545 – 1553, July 2011.

[5] S. M. Brahma, A. A. Girgis, "Development of Adaptive Protection Scheme for Distribution Systems with High Penetration of Distributed Generation," IEEE Trans. Power Delivery, Vol. 19-1, pp. 56-63, January 2004.

[6] O. A. S. Youssef, "Combined fuzzy-logic wavelet-based fault classification technique for power system relaying," Power Delivery, IEEE Trans. on, vol. 19, no. 2, pp. 582-589, Apr 2004.

[7] F. B. Costa, B. A. Souza and N. S. D. Brito, "Real-time classification of transmission line faults based on Maximal Overlap Discrete Wavelet Transform," in Transmission and Distribution Conference and Exposition (T&D), 2012 IEEE PES, Orlando, FL, May 2012.

[8] A. M. Gaouda, S. H. Kanoun, M. M. Salama and A. Y. Chikhani, "Pattern recognition applications for power system disturbance classification," Power Delivery, IEEE Trans. on, vol. 17, no. 3, pp. 677-683, Jul 2002.

[9] S. Santoso, W. M. Grady, E. J. Powers, J. Lamoree and S. C. Bhatt, "Characterization of distribution power quality events with Fourier and wavelet transforms," Power Delivery, IEEE Trans. on, vol. 15, no. 1, pp. 247-254, Jan 2000.

[10] Santoso, S.; Powers, E.J.; Grady, W.M.; Hofmann, P., "Power quality assessment via wavelet transform analysis," Power Delivery, IEEE Trans. on , vol.11, no.2, pp. 924-930, Apr 1996.

[11] C. M. Schegan, "A hardware/software platform for fault detection and identification in electric power distribution systems for testing various detection schemes," M.S. Thesis, Dept. of Elec. and Comp. Eng., Drexel Univ., Philadelphia, PA, 2008.

[12] P. Pillay and A. Bhattacharjee, "Application of wavelets to model short-term power system disturbances," Power Systems, IEEE Trans. on, vol. 11, no. 4, pp. 2031-2037, Nov 1996.

[13] X. Yang, C. Bruni, D. Cheung, Y. Mao, G. Sokol, K. Miu and C. Nwankpa, "Setup of RDAC - a reconfigurable distribution automation and control laboratory," in Power Engineering Society Summer Meeting, 2001, Vancouver, BC, 2001.

[14] S. Theodoridis and K. Koutroumbas. Pattern Recognition. Burlington, MA: Elsevier, 2009.

Nicholas S. Coleman (S'2012) received B.S. and M.S. degrees in electrical engineering from Drexel University, Philadelphia, PA, USA, in 2013, where he is currently a Ph.D. candidate.

Christian Schegan (M'2015) received the B.S. (2008), M.S. (2008) and Ph.D. (2015) degrees in electrical engineering from Drexel University. He is currently with the Naval Surface Warfare Center in Philadelphia, PA, USA.

Karen N. Miu (M'1998) received the B.S., M.S., and Ph.D. degrees in electrical engineering from Cornell University, Ithaca, NY, USA. She is currently a Professor in the Electrical and Computer Engineering Department at Drexel University.